

**MAXIMALLY RANDOM SYSTEMS,
MAXIMALLY DEGENERATE ORDERING,
AND
LOWER LOWER-CRITICAL
SPIN-GLASS DIMENSION**

by

BORA ATALAY

Submitted to the Graduate School of Engineering and Natural Sciences
in a partial fulfillment of
the requirements for the degree of
Master of Science

Sabancı University

July 2018

Maximally Random Systems, Maximally Degenerate Ordering,
and Lower Lower-Critical Spin-Glass Dimension

APPROVED BY:

Prof. Dr. A. Nihat Berker
(Thesis Supervisor)



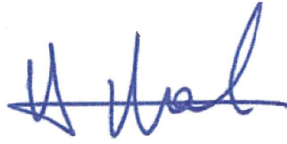
Prof. Dr. Ali Rana Atılgan



Prof. Dr. Cem Güneri



Asst. Prof. Dr. Neşe Aral



Prof. Dr. Zehra Akdeniz



DATE OF APPROVAL: 31.07.2018

© Bora Atalay 2018

All Rights Reserved

ABSTRACT

MAXIMALLY RANDOM SYSTEMS, MAXIMALLY DEGENERATE ORDERING, AND LOWER LOWER-CRITICAL SPIN-GLASS DIMENSION

BORA ATALAY

M.Sc. Dissertation, July 2018

Thesis Supervisor: Prof. A. Nihat Berker

Keywords: Renormalization-group theory, quenched random systems, maximal randomness, maximal degeneracy, mixed-spatial dimensions, lower-critical dimension

Discrete-spin systems with maximally random nearest-neighbor interactions that is symmetric or asymmetric, ferromagnetic or antiferromagnetic, including off-diagonal disorder, are studied, for $q=3,4$ states in d dimensions. Using renormalization-group theory, for all $d \geq 1$ and all noninfinite temperatures, the system eventually renormalizes to a random single state, thus signaling $q \times q$ degenerate ordering, which is maximally degenerate ordering. For high-temperature initial conditions, the system crosses over to this highly degenerate ordering only after spending many renormalization-group iterations near the disordered (infinite-temperature) fixed point. Thus, a temperature range of short-range disorder in the presence of long-range order is identified, as previously seen in underfrustrated Ising spin-glass systems. The entropy behaves similarly for ferromagnetic and antiferromagnetic interactions, and shows a derivative maximum at the short-range disordering temperature. As expected, the system is disordered at all temperatures for $d = 1$.

By quenched-randomly mixing local units of different spatial dimensionalities, we also have studied Ising spin-glass systems on hierarchical lattices continuously in dimensionalities $1 \leq d \leq 3$. The global phase diagram in temperature, antiferromagnetic bond concentration, and spatial dimensionality is calculated. We found, the spin-glass phase disappears to zero temperature at the lower-critical dimension $d_c = 2.431$. This sets an upper limit to the lower-critical dimension in general for the Ising spin-glass phase. As dimension is lowered towards d_c , the spin-glass critical temperature continuously goes to zero, but the spin-glass chaos fully sustains to the brink of the disappearance of the spin-glass phase. The Lyapunov exponent, measuring the strength of chaos, is thus largely unaffected by the approach to d_c and shows a discontinuity to zero at d_c .

ÖZET

AZAMI RASTGELE SİSTEMLER, AZAMI YOZ DÜZENLEŞİM, VE DÜŞÜK ALTKRİTİK SPİN-CAMI BOYUTU

BORA ATALAY

Yüksek Lisans Tezi, Temmuz 2018

Tez Danışmanı: Prof. A. Nihat Berker

Anahtar Kelimeler: Renormalizasyon-grup teorisi, donmuş rastgele sistemler, azami rastgelelilik, azami yozluk, birleştirilmiş uzamsal boyutlar, altkritik boyut.

Simetrik veya asimetrik, ferromanyetik veya antiferromanyetik en yakın komşu etkileşimlerinin azami ölçüde rastgele olduğu kesikli-spin sistemleri, köşegen dışı düzensizlik de dahil edilerek, $q=3,4$ durum için d boyutta incelendi. İncelememizde hiyerarşik örgüler için tam ve hiperkübik örgüler için yaklaşık (Migdal-Kadanoff) olan renormalizasyon-grup teorisi kullanıldı. Bulgularımıza göre böyle sistemler tüm $d \geq 1$ boyutlar ve sonsuz olmayan sıcaklıklar için nihayetinde tek bir rastgele duruma renormalize olarak $q \times q$ yoz düzenleme oluşturuyor. Dikkat ediniz ki bu azami ölçüde yoz düzenleştirmedir. Yüksek sıcaklıktaki başlangıç koşullarında, sistem ancak nice renormalizasyon-grup iterasyonunu düzensiz (sonsuz-sıcaklık) sabit noktası (fixed point) civarında geçirdikten sonra azami yoz düzenleme doğru yöneliyor. Dolayısıyla, altbunalımlı Ising spin-camlarında da görülen, uzun-menzilli düzenlilik yapısı altında kısa-menzilli düzensizliğe ait bir sıcaklık menzili bulunmuştur. Tüm sıcaklıklar için entropi hesaplanmış olup, ferromanyetik ve antiferromanyetik sistemlerde entropinin eş davranışlı olduğu, ve kısa-menzilli düzensizlik sıcaklığında bir türev maksimumuna sahip olduğu bulunmuştur. Sistem, $1 + \epsilon$ boyut için bariz bir zıtlıkla birlikte, $d = 1$ boyut için beklenildiği gibi her sıcaklıkta düzensiz durumdadır.

Ayrıca, farklı uzamsal boyutluluklardaki bölgesel birimler donmuş rastgelelilikle birbirine bağdaştırılarak, Ising spin-camları $1 \leq d \leq 3$ sürekli boyutlarındaki hiyerarşik örgülerde incelendi. Sıcaklık, antiferromanyetik bağ yoğunluğu, ve uzamsal boyutluluk cinsinden genel faz diyagramı hesaplandı. Bulgularımıza göre, spin-camı fazı sıfır sıcaklıkta $d_c = 2.431$ altkritik boyutunda ortadan kalkıyor. Sistemimiz fiziksel anlamda gerçekleşir bir sistem olduğundan, bu bulgu genel anlamda Ising spin-camı fazı için altkritik boyuta bir üst limit koymuştur. Boyut, d_c altkritik boyutuna doğru azaldıkça spin-camı kritik sıcaklığı sıfıra sürekli olarak yaklaşırken, spin-camı kaosu spin-camı fazı ortadan kalkana dek devam etmektedir. Dolayısıyla, kaosun güç ölçeği olan Lyapunov üsteli d_c boyutuna yakınlardan pek etkilenmemekte, ve d_c boyutunda süresizlikle sıfıra inmektedir.

ACKNOWLEDGEMENTS

This work is a result of many enduring and concurrently endearing times in my graduate studies in physics. I feel such an honor and gratitude for moulding those times with my advisor Prof. A. Nihat Berker. With his fervor for excellence, meticulous work ethic, and timely friendship I have learned a lot.

I thank Efe İlker and Tolga Çağlar for helping me in the very early days of my time in the studies of phase transitions. I am also thankful to Tolga for his insight and boot camp in computational physics.

My deepest thoughts go for my grandmother who has merely seen the morning of this work.

I thank for my family for their everlasting love and support, my cat Limon for her pluckiness, and my longtime friend Berk Aydın firstly for his friendship, his trailblazing nature, and for riposting together against many.

TABLE OF CONTENTS

1	INTRODUCTION	1
2	MAXIMALLY RANDOM DISCRETE-SPIN SYSTEMS WITH SYMMETRIC AND ASYMMETRIC INTERACTIONS AND MAXIMALLY DEGENERATE ORDERING	2
2.1.	Introduction: Asymmetric and Symmetric Maximally Random Spin Models	2
2.2.	Renormalization-Group Transformation	4
2.3.	Asymptotically Dominant All-Temperature Freezing in $d > 1$ with High-Temperature Short-Range Disordering	5
2.4.	Free Energy, Entropy, and Specific Heat	7
2.5.	Antiferromagnetic Maximally Random Systems	10
2.6.	Conclusion	10
3	A LOWER LOWER-CRITICAL SPIN-GLASS DIMENSION FROM QUENCHED MIXED-SPATIAL DIMENSIONAL SPIN GLASSES	11
3.1.	Introduction	11
3.2.	Model and Method: Moving between Spatial Dimensions through Local Differentiation	13
3.3.	Transitional Dimensional Global Phase Diagram and Full Chaos Even at Spin-Glass Disappearance	16
3.4.	Conclusion	18
4	CONCLUSION	19

LIST OF FIGURES

2.1	Renormalization-group trajectories for the system with $q = 3$ states in $d = 3$ dimensions	6
2.2	Calculated free energy per bond as a function of temperature $T = J^{-1}$	8
2.3	Calculated entropy per bond as a function of temperature $T = J^{-1}$, for $q = 3, 4$ states in $d = 3, 4$ dimensions.	9
2.4	Calculated specific heat as a function of temperature $T = J^{-1}$, for $q = 3, 4$ states in $d = 3, 4$ dimensions.	9
2.5	Calculated specific heat as a function of temperature $T = J ^{-1}$ for ferromagnetic ($J > 0$), full curves, and antiferromagnetic ($J < 0$), dashed curves, systems, for $q = 3, 4$ states in $d = 3, 4$ dimensions.	10
3.1	Local graphs with $d = 2$ (bottom) and $d = 3$ (top) connectivity.	12
3.2	Calculated exact global phase diagram of the Ising spin glass on the cross-dimensional hierarchical lattice, in temperature $1/J$, antiferromagnetic bond concentration p , and spatial dimension d	13
3.3	Constant dimensionality d cross sections of the global phase diagram in Fig. 3.2.	14
3.4	Zero-temperature phase diagram of the Ising spin glass on the cross-dimensional hierarchical lattice, in antiferromagnetic bond concentration p and and spatial dimension d	15
3.5	The chaotic renormalization-group trajectory of the interaction J_{ij} at a given location $\langle ij \rangle$, for various spatial dimensions between the lower-critical $d_c = 2.431$ and $d = 3$	17
3.6	Spin-glass critical temperature T_C^{SG} at $p = 0.5$, spin-glass chaos Lyapunov exponent λ , spin-glass-phase runaway exponent y_R^{SG} and ferromagnetic-phase runaway exponent y_R^F , as a function of dimension d	18

Chapter 1

INTRODUCTION

Spin-glasses can be nonchalantly expressed as a type of disordered magnetic systems where its constituents have an irregular magnetic spin alignment. That being said, while the studies on spin-glasses and critical phenomena not only enabled the development of thriving theoretical and numerical techniques with which we understand the physics of such systems better, these techniques turned out to have far reaching applications besides magnetic systems, and boosted the studies on biological evolution, neural networks, machine learning, financial and social systems, and many other complex systems.

In this work we have started from wholesome beginnings and achieved challenging results for discrete-spin systems using renormalization-group theory. In the first study, we allowed each spin site to randomly favor one of the available states for its interaction with a nearest neighbor, thereby allowing the system to form both asymmetric and symmetric interactions and enabling maximal randomness throughout the system. In the second study, by quenched-randomly mixing local units of different spatial dimensionalities, we have studied Ising spin-glass systems, chaotic behavior, and emergence of spin-glass phase on hierarchical lattices in continuous dimensionalities. Both works demonstrate the versatility of renormalization-group theory in pursuit of solving physical systems. Although the results we obtain here are most general in itself, our approach and setting have a room for further development in systems with different Hamiltonians.

Chapter 2

MAXIMALLY RANDOM DISCRETE-SPIN SYSTEMS WITH SYMMETRIC AND ASYMMETRIC INTERACTIONS AND MAXIMALLY DEGENERATE ORDERING

2.1. Introduction: Asymmetric and Symmetric Maximally Random Spin Models

Spin models such as Ising, Potts, ice models show a richness of phase transitions and multicritical phenomena [1, 2] that is qualitatively compounded with the addition of frozen (quenched) randomness. Examples are the emerging chaos in spin glasses with competing ferromagnetic and antiferromagnetic (and more recently, without recourse to ferromagnetism vs. antiferromagnetism, competing left and right chiral [3]) interactions, the conversion of first-order phase transitions to second-order phase transitions, and the infinite multitude of accumulating phases as devil's staircases. In the current study, frozen randomness is taken to the limit, in $q = 3, 4$ state models in arbitrary dimension d and the results are quite unexpected. Thus, changes in the critical properties and the phase-transition order are the effects quenched randomness, as well as the appearance of new phenomena such as chaotic rescaling and devil's staircase topologies of phase diagrams. A key microscopic ingredient in these phenomena is the occurrence of frustration, in which

all interactions along closed paths in the lattice cannot be simultaneously satisfied. The renormalization-group transformation that we use in this study is equipped to study frustrated systems (and thus has been extensively used in spin-glass systems), as can be seen below by from the equivalent hierarchical lattice where closed loops occur corresponding to bond-moving following decimation. The systems that we study are quenched maximally random q -state discrete spin models with nearest-neighbor interactions, with Hamiltonian

$$-\beta\mathcal{H} = - \sum_{\langle ij \rangle} \beta\mathcal{H}_{ij}, \quad (2.1)$$

where the sum is over nearest-neighbor pairs of sites $\langle ij \rangle$.

The maximal randomness is best expressed in the transfer matrix T_{ij} , e.g., for $q = 3$,

$$\mathbf{T}_{ij} \equiv e^{-\beta\mathcal{H}_{ij}} = \begin{pmatrix} 1 & e^J & 1 \\ 1 & 1 & e^J \\ e^J & 1 & 1 \end{pmatrix}, \begin{pmatrix} 1 & 1 & e^J \\ e^J & 1 & 1 \\ 1 & e^J & 1 \end{pmatrix}, \begin{pmatrix} e^J & 1 & 1 \\ 1 & 1 & e^J \\ 1 & e^J & 1 \end{pmatrix}, \\ \begin{pmatrix} 1 & 1 & e^J \\ 1 & e^J & 1 \\ e^J & 1 & 1 \end{pmatrix}, \begin{pmatrix} 1 & e^J & 1 \\ e^J & 1 & 1 \\ 1 & 1 & e^J \end{pmatrix}, \text{ or } \begin{pmatrix} e^J & 1 & 1 \\ 1 & e^J & 1 \\ 1 & 1 & e^J \end{pmatrix}, \quad (2.2)$$

where each row and each column has, randomly, a single e^J element, so that there are 6 such possibilities (for $q = 4$, also studied here, there are 24 such possibilities), and $J > 0$ or $J < 0$ respectively for ferromagnetic or antiferromagnetic interactions, both of which are treated in this study. The last matrix corresponds to the usual Potts model. In fact, taken by itself as a pure (non-random) model, each of these transfer matrices can be mapped to a Potts model by relabeling the spin states in one of the two sublattices, in hypercubic lattices and corresponding hierarchical lattices. Thus, for the ferromagnetic case, for $d > 1$, a low-temperature ferromagnetic phase and a high-temperature disordered phase occurs. For the antiferromagnetic case, the low-temperature phase is a critical phase and appears at a higher dimension.[4, 5]

In Hamiltonian terms, the currently studied, quenched random model is

$$-\beta\mathcal{H}_{i,j} = J\delta_{\sigma_i, P(\sigma_j)}, \quad (2.3)$$

where P is a random permutation of $\{a, b, c\}$. Thus, at a given site i , for a given spin state, say $s_i = a$, randomly any one of the spin states $s_j = a, b$, or c of the nearest-neighbor site j is energetically favored (unfavored) for ferromagnetic (antiferromagnetic) interactions. This favor (unfavor) is independently random for each of the nearest-neighbors j . Under renormalization-group transformation, all elements of the transfer matrices across the system randomize. Therefore, we have not included in our renormalization-group initial conditions the cases where there is a difference between the less favored two states, to keep the enunciation of the model simple. However, since our renormalization-group trajectories traverse the latter states, we are confident that our results will not be affected by such a sub-discrimination.

The first two possible transfer matrices on the right side of Eq.(2.2) represent asymmetric interaction, in the sense that the nearest-neighbor states $(s_i, s_j) = (a, b)$ and (b, a) have different energies, where $s_i = a, b$, or c are the $q = 3$ possible states of a given site i . Asymmetric interactions occur in neural network systems [6] and are largely unexplored in statistical mechanics. On the other hand, the last four possible transfer matrices on the right side of Eq.(2.2) exemplify symmetric interaction, the nearest-neighbor states $(s_i, s_j) = (a, b)$ and (b, a) having the same energies. As also explained below, even when starting with only symmetric interactions (the last four matrices), asymmetric interactions are generated under renormalization-group transformations (as can be seen, e.g. by multiplying the third and fifth matrices in Eq.(2.2), corresponding to a renormalization-group decimation) and the same ordering results are obtained. Thus, asymmetric interactions are generated by off-diagonal (symmetric) disorder. The generalization of the above model to arbitrary q is obvious.

2.2. Renormalization-Group Transformation

The renormalization-group method is readily implemented to the transfer matrix form of the interactions. The quenched randomness aspect of the problem is included by randomly creating 500 transfer matrices from the 6 possibilities of Eq.(2.2) and perpetuating these random 500 transfer matrices throughout the renormalization-group steps given below. Note that we start with a single initial value of J , which is proportional to the inverse temperature. Quenched randomness comes from the positioning within the matrix.

Under renormalization-group transformation, each matrix element evolves quantitatively quenched randomly.

The renormalization-group transformation begins by the "bond-moving" step in which b^{d-1} transfer matrices, each randomly chosen from the 500, have their corresponding matrix elements multiplied. This operation is repeated 500 times, thus generating 500 new transfer matrices. The final, "decimation" step of the renormalization-group transformation is the matrix multiplication of b transfer matrices, again each randomly chosen from the 500. This operation is also repeated 500 times, again generating 500 renormalized transfer matrices. The length rescaling factor is taken as $b = 2$ in our calculation. At each transfer-matrix calculation above, each element of the resulting transfer matrix is divided by the largest element, resulting in a matrix with the largest element being unity. This does not affect the physics, since it corresponds to subtracting a constant from the Hamiltonian. These subtractive constants (the natural logarithm of the dividing element) are scale-accumulated, as explained below, for the calculation of entropy.

The above transformation is the approximate Migdal-Kadanoff [7, 8] renormalization-group transformation for hypercubic lattices and, simultaneously, the exact renormalization-group transformation of a hierarchical lattice [9, 10, 11]. This procedure has been explained in detail in previous works.[3] For most recent exact calculations on hierarchical lattices, see Ref.[12, 13, 14, 15, 16, 17, 18, 19], including finance [18] and DNA-binding [19] problems.

2.3. Asymptotically Dominant All-Temperature Freezing in $d > 1$ with High-Temperature Short-Range Disorder

Figure 1.1 shows the renormalization-group trajectories for the system with $q = 3$ states in $d = 3$ dimensions, starting at three different temperatures $T = J^{-1}$, where J refers to the renormalization-group-trajectory initial conditions shown in Eqs.(2.2,2.3). Shown are the second (J_2) and third (J_3) largest values of the energies (dimensionless, being temperature-divided) that appear exponentiated in the transfer matrix elements,

$$J_{ij} = \ln(T_{ij}), \tag{2.4}$$

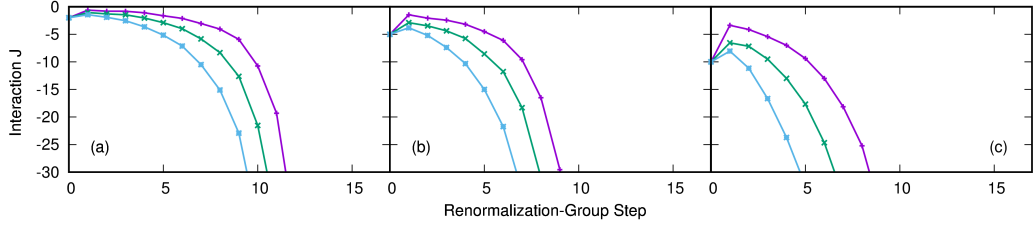


Figure 2.1: Renormalization-group trajectories for the system with $q = 3$ states in $d = 3$ dimensions, starting at three different temperatures $T = J^{-1}$ from Eqs.(2.2,2.3), namely starting with (a) $J = 0.02$, (b) $J = 0.20$, (c) $J = 0.50$. Shown are the second (J_2), third (J_3) largest values and the matrix average of the eight non-leading energies $\langle J_{2-9} \rangle$ of the transfer matrix (Eq.(2.4)), averaged over the quenched random distribution. The leading energy is $J_1 = 0$ by subtractive choice. The different starting values can be seen on the left axis of each panel (corresponding to renormalization-group step 0). Starting at any non-zero temperature, the system renormalizes to a state in which the leading energy is totally dominant, all other energies renormalizing to $-\infty$. The matrix position of the single asymptotically dominant element occurs randomly among the $q \times q$ possibilities including off-diagonal and therefore necessarily asymmetric, but is the same across the quenched random distribution. However, starting at high temperatures, as seen e.g. in the left and center panels in this figure, the system spends many renormalization-group iterations near the infinite-temperature fixed point (where all energies are zero), before crossing over to the ordered fixed point. Since the energies at a specific step of a renormalization-group trajectory directly show the effective couplings across the length scale that is reached at that renormalization-group step, this behavior indicates islands of short-range disorder at the short length scales that correspond to the initial steps of a renormalization-group trajectory. These islands of short-range disorder nested in long-range order have been explicitly calculated and shown in spin-glass systems in Ref. (20). These islands of short-range disorder occur in the presence of long-range order, since the trajectories eventually flow to the strong-coupling fixed point. As temperature is increased (changing the renormalization-group initial condition), these short-range disordered regions order, giving rise to the smooth specific heat peak, but no phase transition singularity, as there is no additional fixed-point structure underlying this short-range ordering.

averaged over the quenched random distribution, where T_{ij} are the elements of the $q \times q$ transfer matrix \mathbf{T}_{ij} . The matrix average of the eight non-leading energies $\langle J_{2-9} \rangle$, averaged over the quenched random distribution, is also shown. The leading energy is $J_1 = 0$ by subtractive overall constant, as explained above. As seen in this figure, starting at low temperature $T = 2$, the system renormalizes to a state in which the leading energy is totally dominant, all other energies renormalizing to $-\infty$. The matrix position of the single asymptotically dominant element occurs randomly among the $q \times q$ possibilities including off-diagonal and therefore necessarily asymmetric, but is the same across the quenched random distribution. The number of possible dominant transfer-matrix elements gives the degeneracy of the ordered phase, so that with $q \times q$, maximal degeneracy is achieved. A diagonal element of the transfer matrix being dominant means that one state, e.g. $s_i = c$ dominates at the strong coupling fixed point and characterizes the ordered phase. This does not have the usual permutational symmetry of the Potts model, being physically equivalent to all diagonal elements dominating, but with non-diagonal elements zero so that only one spin state dominates the entire physical system. The equivalence is not complete only

in the fact that the latter picture allows different domains in the system, where as the former does not. A non-diagonal element $T_{km} = 1$ being dominant maintains itself by having T_{im}, T_{kj} , where $i \neq k, j \neq m$, being small, decreasing under renormalization-group, but non-zero. The corresponding spin state is highly degenerate, as can be seen from the renormalization-group solution, where each spin has a degeneracy of 2 (still less than the disordered number of q), seen at decimation transformations, and the system is randomly populated by two spin states corresponding to the indices k and m of the dominant T_{km} . Moreover, starting at high temperatures, as seen e.g. in the left and center panels of Fig. 2.1, the system spends many renormalization-group iterations near the infinite-temperature fixed point (where all energies are zero), before crossing over to the ordered fixed point. This signifies short-range disorder, in the presence of long-range order, as also reflected in the specific heat peaks caused by short-range disordering as discussed below. A similar smeared transition to short-range disorder in the presence of long-range order has previously been seen in underfrustrated Ising spin-glass systems.[22]

We have repeated our calculations for non-integer spatial dimensions approaching $d = 1$ from above, by keeping the bond-moving number $b^{d-1} = 2$ and increasing the decimation number b . The behavior described above obtains for all $d \gtrsim 1$, albeit with an increasing high-temperature range of short-range disorder, and higher number of renormalization-group steps to strong coupling, as $d = 1$ is approached. At $d = 1$, the infinite-temperature fixed point is the sole attractor and the system is disordered at all temperatures.

2.4. Free Energy, Entropy, and Specific Heat

The renormalization-group solution gives the complete equilibrium thermodynamics for the systems studied. The dimensionless free energy per bond $f = F/kN$ is obtained by summing the additive constants generated at each renormalization-group step,

$$f = \frac{1}{N} \ln \sum_{\{s_i\}} e^{-\beta\mathcal{H}} = \sum_{n=1} \frac{G^{(n)}}{b^{dn}}, \quad (2.5)$$

where N is the number of bonds in the initial unrenormalized system, the first sum is over all states of the system, the second sum is over all renormalization-group steps n , $G^{(n)}$ is the additive constant generated at the (n) th renormalization-group transformation averaged over the quenched random distribution, and the sum quickly converges numerically.

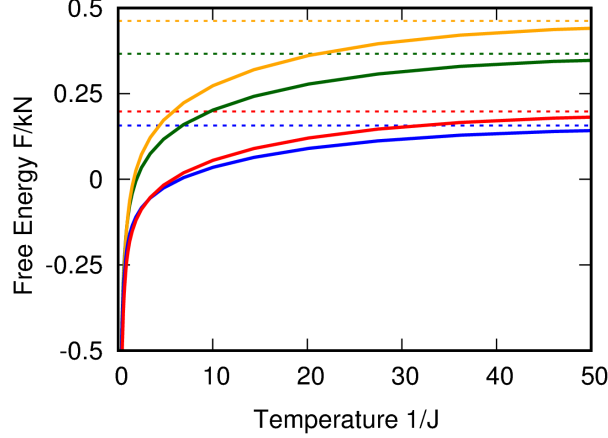


Figure 2.2: Calculated free energy per bond as a function of temperature $T = J^{-1}$. The curves are, from top to bottom, for $(q = 4, d = 2)$, $(q = 3, d = 2)$, $(q = 4, d = 3)$, $(q = 3, d = 3)$. The expected $T = \infty$ values of $f = F/kN = \ln q/(b^d - 1)$ are given by the dashed lines and match the calculations.

From the dimensionless free energy per bond f , the entropy per bond S/kN is calculated as

$$\frac{S}{kN} = f - J \frac{\partial f}{\partial J} \quad (2.6)$$

and the specific heat C/kN is calculated as

$$\frac{C}{kN} = T \frac{\partial(S/kN)}{\partial T} = -J \frac{\partial(S/kN)}{\partial J}. \quad (2.7)$$

Figures 2.2-2.4 give the calculated free energies f , entropies S/kN , and specific heats C/kN per bond as functions of temperature $T = J^{-1}$, for $q = 3, 4$ states in $d = 3, 4$ dimensions. The expected $T = \infty$ values of $f = \ln q/(b^d - 1)$ and $S/kN = \ln q/(b^d - 1)$ are given by the dashed lines and match the calculations.

As explained in Fig. 2.1, the specific heat maximum occurs at the temperature of the short-range disordering. In this figure, starting at high temperatures, as seen e.g. in the left and center panels in this figure, the system spends many renormalization-group iterations near the infinite-temperature fixed point (where all energies are zero), before crossing over to the ordered fixed point. Since the energies at a specific step of a renormalization-group trajectory directly show the effective couplings across the length scale that is reached at that renormalization-group step, this behavior indicates islands of short-range disorder at the short length scales that correspond to the initial steps of a renormalization-group trajectory. These islands of short-range disorder nested in long-range order have been explicitly calculated and shown in spin-glass systems in Ref. (20). These islands of short-

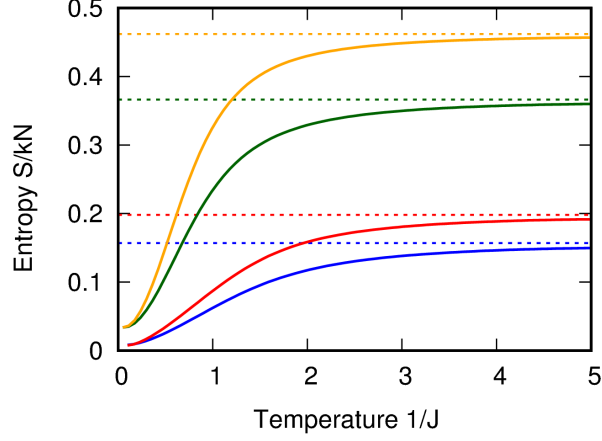


Figure 2.3: Calculated entropy per bond as a function of temperature $T = J^{-1}$, for $q = 3, 4$ states in $d = 3, 4$ dimensions. The curves are, from top to bottom, for $(q = 4, d = 2)$, $(q = 3, d = 2)$, $(q = 4, d = 3)$, $(q = 3, d = 3)$. The expected $T = \infty$ values of $S/kN = \ln q/(b^d - 1)$ are given by the dashed lines and match the calculations.

range disorder occur in the presence of long-range order, since the trajectories eventually flow to the strong-coupling fixed point. As temperature is increased (changing the renormalization-group initial condition), these short-range disordered regions order, giving rise to the smooth specific heat peak, but no phase transition singularity, as there is no additional fixed-point structure underlying this short-range ordering. Specific heat maxima away from phase transitions, due to short-range ordering, have been calculated in a variety of systems [21, 22].

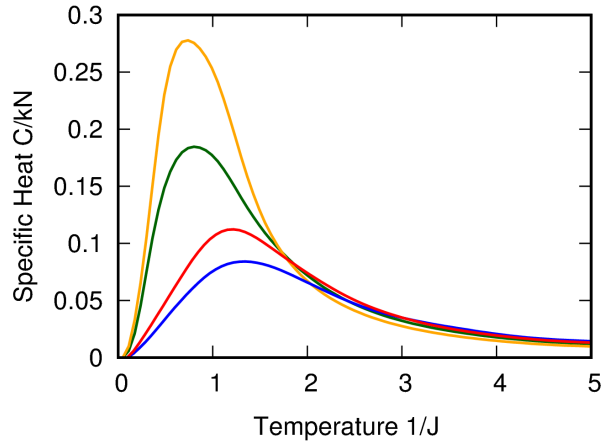


Figure 2.4: Calculated specific heat as a function of temperature $T = J^{-1}$, for $q = 3, 4$ states in $d = 3, 4$ dimensions. The curves are, from top to bottom, for $(q = 4, d = 2)$, $(q = 3, d = 2)$, $(q = 4, d = 3)$, $(q = 3, d = 3)$. A specific heat maximum occurs at short-range disordering.

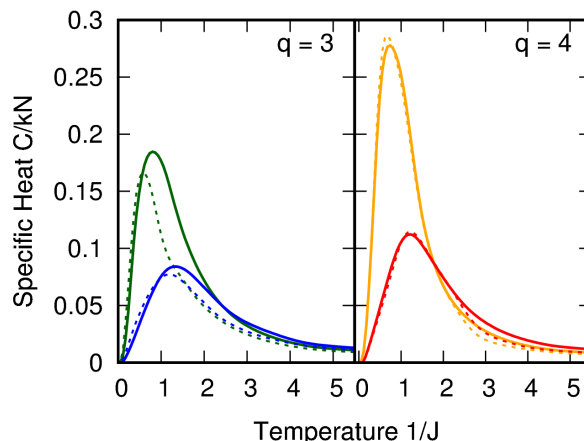


Figure 2.5: Calculated specific heat as a function of temperature $T = |J|^{-1}$ for ferromagnetic ($J > 0$), full curves, and antiferromagnetic ($J < 0$), dashed curves, systems, for $q = 3, 4$ states in $d = 3, 4$ dimensions. The curves are, from top to bottom in each panel, for $d = 2$ and $d = 3$. The quantitatively same short-range disordering behavior is seen for both ferromagnetic and antiferromagnetic systems.

2.5. Antiferromagnetic Maximally Random Systems

We have repeated our calculations for antiferromagnetic ($J < 0$) systems and obtained quantitatively similar behavior. Fig. 2.5 shows the calculated specific heats as a function of temperature $T = |J|^{-1}$ for ferromagnetic ($J > 0$) and antiferromagnetic ($J < 0$) systems, for $q = 3, 4$ states in $d = 3, 4$ dimensions. The full-temperature range ($T < -\infty$) maximally degenerate long-range ordering and a quantitatively same short-range disordering at high temperature is seen for both ferromagnetic and antiferromagnetic systems.

2.6. Conclusion

We have studied maximally random discrete-spin systems with symmetric and asymmetric interactions and have found, quite surprisingly, (1) quenched random long-range order at all non-infinite temperatures for $d > 1$, (2) short-range disordering at high temperatures, via a smeared transition and a specific-heat peak, while sustaining long-range order. The latter behavior has also been seen in underfrustrated Ising spin-glass systems[22].

Chapter 3

A LOWER LOWER-CRITICAL SPIN-GLASS DIMENSION FROM QUENCHED MIXED-SPATIAL DIMENSIONAL SPIN GLASSES

3.1. Introduction

The lower-critical dimension d_c of an ordering system, where the onset of an ordered phase is seen as spatial dimension d is raised, has been of interest as a singularity of a continuous sequence of singularities, the latter being the phase transitions to the ordered phase which change continuously as d is raised from d_c . The lower-critical dimension of systems without quenched randomness has been known for some time as $d_c = 1$ for the Ising-type ($n = 1$ component order-parameter) systems, $d_c = 2$ for XY, Heisenberg, ... ($n = 2, 3, \dots$) systems, highlighted with a temperature range of criticality at $d_c = 2$ of the XY model [23, 24]. In systems with quenched randomness, a marvelous controversy on the lower-critical dimension of random-field Ising system has settled for $d_c = 2$. [25, 26, 27, 28, 29, 30, 31, 32] Quenched bond randomness affects the first- versus second-order nature of the phase transition into an ordered phase that exists without quenched randomness (such as the ferromagnetic phase), rather than the dimensional onset of this ordered phase.

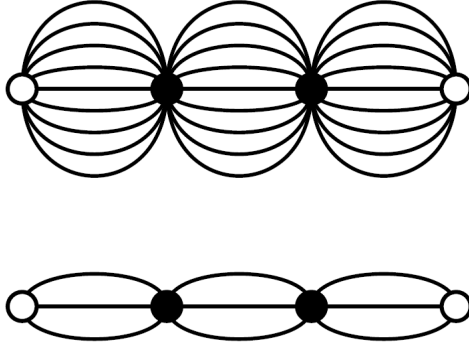


Figure 3.1: Local graphs with $d = 2$ (bottom) and $d = 3$ (top) connectivity. The cross-dimensional hierarchical lattice is obtained by repeatedly imbedding the graphs in place of bonds, randomly with probability $1 - q$ and q for the $d = 2$ and $d = 3$ units, respectively.

The situation is inherently different with an ordered phase that is caused by the quenched randomness of competing ferromagnetic-antiferromagnetic (and more recently right-left chirality or helicity [3]) interactions, namely the Ising spin-glass phase. Replica-symmetry-breaking mean-field theory yields $d_c = 2.5$ [33] this being of immediate high interest as the first known example of a non-integer lower-critical dimension. Numerical fit to spin-glass critical temperatures [34] and free energy barriers [35] for integer dimensions also suggests $d_c = 2.5$. Numerical fits to the exact renormalization-group solutions of two different families of hierarchical lattices with a sequence of decreasing dimensions yield $d_c = 2.504$ [36, 37] and $d_c = 2.520$ [38], which are of further interest by being non-simple fractions. The strength of hierarchical lattice approaches is that they present exact (numerical) solutions [9, 10, 11], but they involve non-unique continuations between integer dimensions, being based on different families of fractal graphs. However, in the hunt for the lower-critical dimension, since each hierarchical lattice constitutes a physical realization, calculating a finite-temperature spin-glass phase at d automatically pushes the lower-critical dimension to $d_c < d$, which is an important piece of information. The exact numerical renormalization-group solution of hierarchical lattices, used in the current study, has been fully successful in all aspects of lower-critical-dimension behavior mentioned in the first paragraphs of this Section. Whereas previous studies with hierarchical lattices have used in each calculation a lattice with the same dimensionality at every locality (these include but are not confined to hierarchical lattices that are simultaneously approximate solutions [7, 8] for hypercubic and other Euclidian lattices), we quenched randomly mix units with local dimensionality $d = 2$ and $d = 3$. By varying the relative concentration of these two units, we continuously span from $d = 2$ to $d = 3$. In this phys-

ically realized system, we find $d_c = 2.431$, lower than previously found values and thus setting an upper limit to the actual lower-critical dimension of the Ising spin-glass phase.

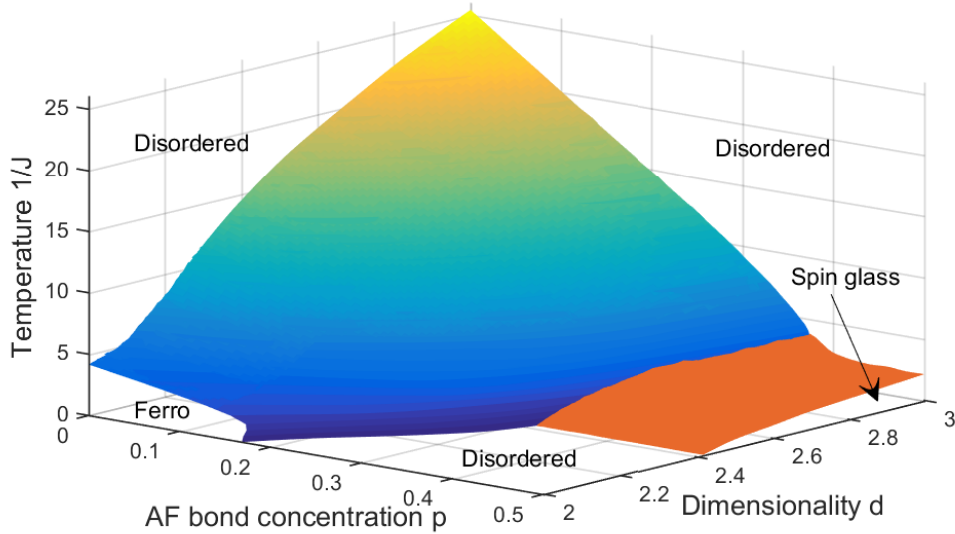


Figure 3.2: Calculated exact global phase diagram of the Ising spin glass on the cross-dimensional hierarchical lattice, in temperature $1/J$, antiferromagnetic bond concentration p , and spatial dimension d . The global phase diagram being symmetric about $p = 0.5$, the mirror image portion of $0.5 < p < 1$ is not shown. The spin-glass phase is thus clearly seen, taking off from zero temperature at $d_c = 2.43$.

Furthermore, as our spin-glass phase disappears at zero-temperature at $d_c = 2.431$, it is fully chaotic, with a calculated Lyapunov exponent of $\lambda = 1.56$ (this exponent equals 1.93 at $d = 3$), which is in sharp contrast to the disappearance, as frustration is microscopically turned off, of the spin-glass phase to the Mattis-gauge-transformed ferromagnetic phase, where the Lyapunov exponent (and chaos) continuously goes to zero[22]. In the current work, we also obtain a global phase diagram in the variables of temperature, antiferromagnetic bond concentration, and spatial dimensionality.

3.2. Model and Method: Moving between Spatial Dimensions through Local Differentiation

The Ising spin-glass system has Hamiltonian

$$-\beta\mathcal{H} = \sum_{\langle ij \rangle} J_{ij} s_i s_j \quad (3.1)$$

where $\beta = 1/kT$, at each site i of the lattice the spin $s_i = \pm 1$, and $\langle ij \rangle$ denotes summation over all nearest-neighbor site pairs. The bond J_{ij} is ferromagnetic $+J > 0$ or antiferromagnetic $-J$ with respective probabilities $1 - p$ and p .

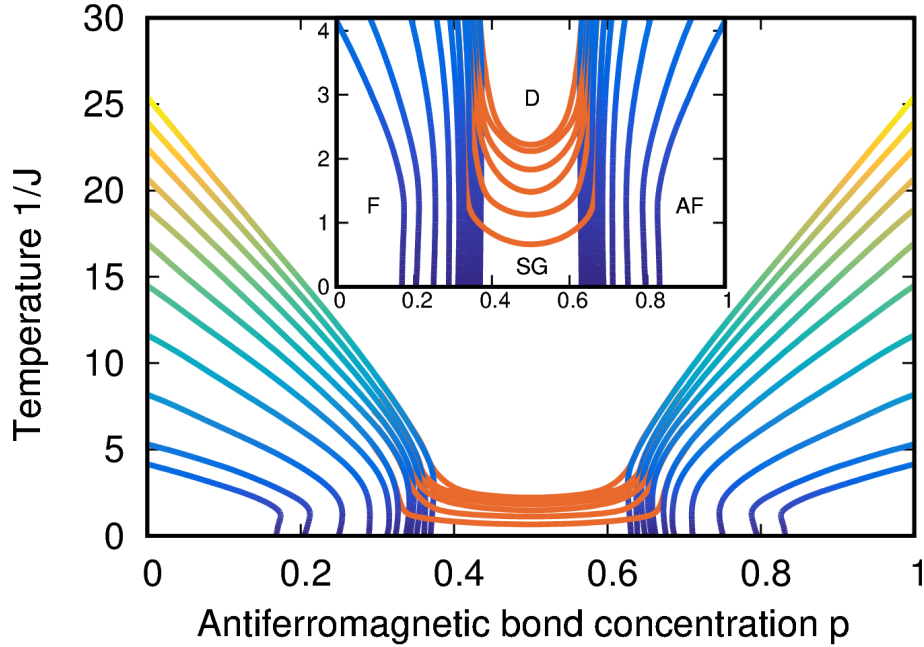


Figure 3.3: Constant dimensionality d cross sections of the global phase diagram in Fig. 3.2. The cross sections are, starting from high temperature, for $d = 3, 2.9, 2.8, 2.7, \dots, 2.1, 2$. It is seen that, as the dimensionality d approaches d_c from above, the spin-glass phase disappears at zero temperature.

This Hamiltonian is lodged on the hierarchical lattice constructed with the two graphs shown in Fig. 3.1. The lower graph has a length rescaling factor (distance between the external vertices) of $b = 3$ and a volume rescaling factor (number of internal bonds) of $b^d = 9$. Thus, self-embedding the lower graph into its bonds *ad infinitum* results in a $d = 2$ spatial dimensional lattice that is numerically exactly soluble. The upper graph similarly yields $d = 3$. Other graphs can be used to systematically obtain intermediate non-integer dimensions.

For recent exact calculations on hierarchical lattices, see Refs.[12, 13, 14, 15, 16, 18, 19, 39, 40]. Thus, previous works have generally used a hierarchical lattice generated by a single graph and spatial dimensionality that is microscopically uniform throughout the system. By contrast, we mix the two graphs with local $d = 2$ and $d = 3$ in frozen randomness and definite proportionality: Starting with either graph (in the thermodynamic limit, this choice does not matter), each bond is replaced by the $d = 2$ or $d = 3$ graph, with probability $1 - q$ and q , respectively. This random imbedding is repeated *ad infinitum*. Thus, the dimensionality of the macroscopic system is $(1 - q) \times 2 + q \times 3 = 2 + q$.

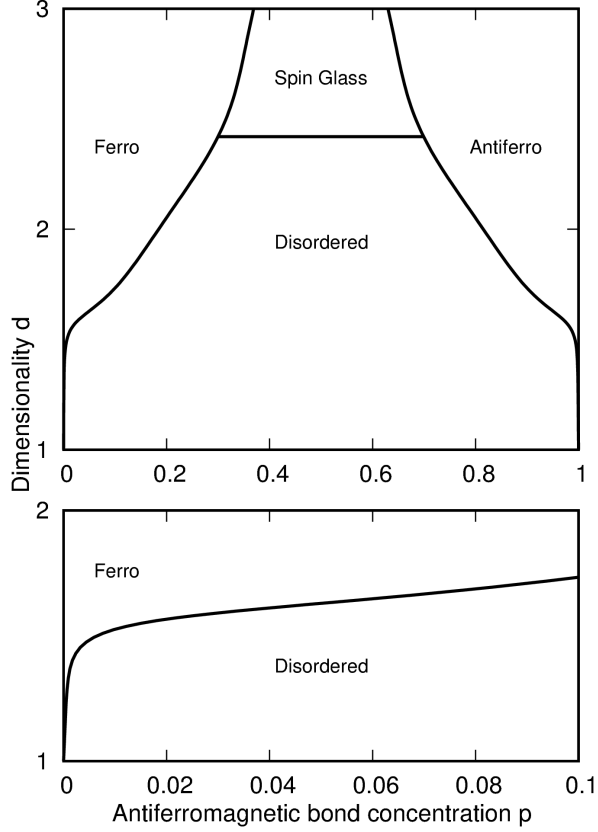


Figure 3.4: Zero-temperature phase diagram of the Ising spin glass on the cross-dimensional hierarchical lattice, in antiferromagnetic bond concentration p and spatial dimension d . The lower-critical dimension of $d_c = 2.431$ is clearly visible.

The exact renormalization-group solution of this system works in the opposite direction from the lattice construction just described. As described after Eq.(2.1), we start with the double-valued distribution of $+J$ or $-J$ bonds, with probabilities $1 - p$ and p respectively, on a $d = 2$ or $d = 3$ unit with probabilities $1 - q$ and q respectively. The local renormalization-group transformation proceeds by b^{d-1} bond-movings followed $b = 3$ (to preserve the ferromagnetic-antiferromagnetic symmetry) decimations, generating a distribution of 500 new interactions, which is of course no longer double valued.[40] (In fact, for numerical efficiency, these operations are broken down to binary steps, each involving two distributions of 500 interactions.) In the disordered phase, the interactions converge to zero. In the ferromagnetic and antiferromagnetic phases, under renormalization-group, the interaction diverges to strong coupling as the renormalized average $\bar{J}' \sim b^{y_R^F} \bar{J}$, where the prime refers to the renormalized system and $y_R^F > 0$ is the runaway exponent of the ferromagnetic sink of the renormalization-group flows. In the spin-glass phase, under renormalization-group, the distribution of interactions continuously broadens symmetri-

cally in ferromagnetism and antiferromagnetism, the absolute value of the interactions diverging to strong coupling as the renormalized average $|\overline{J}|' \sim b^{y_R^{SG}} |\overline{J}|$, where $y_R^{SG} > 0$ is the runaway exponent of the spin-glass sink of the renormalization-group flows. The runaway exponents y_R^F and y_R^{SG} are given below as a function of dimensionality d .

3.3. Transitional Dimensional Global Phase Diagram and Full Chaos Even at Spin-Glass Disappearance

Figure 3.2 shows our calculated global phase diagram in the variables of temperature $1/J$, antiferromagnetic bond concentration p , and spatial dimensionality $2 \leq d \leq 3$. In addition to the high-temperature disordered phase, ferromagnetic, antiferromagnetic (the phase diagram being ferromagnetic-antiferromagnetic symmetric about $p = 0.5$, the mirror-image antiferromagnetic part of $p > 0.5$ is not shown; however, see Figs. 3.3 and 3.4), and spin-glass ordered phases are seen.

As dimensionality d is lowered, the spin-glass phase disappears at zero temperature at the lower-critical dimension of $d_c = 2.431$. Constant-dimension d cross sections of the global phase diagram are in Fig. 3.3, where the gradual temperature-lowering of the spin-glass phase, as the lower-critical dimension $d_c = 2.431$ is approached from above, is seen. However, such gradual disappearance is not the case for the chaos [41, 42, 43] inherent to the spin-glass phase, as seen below. Fig. 3.4 shows the calculated zero-temperature phase diagram in the variables of antiferromagnetic bond concentration p and spatial dimensionality $1 \leq d \leq 3$. For this Figure, the calculation is continuously extended down to $d = 1$ by again quenched-randomly mixing our $d = 2$ graph (Fig. 3.1) and a linear 3-segment strand. The smoothness of the boundaries at $d = 2$ validates our method. The independence of d_c from p is noteworthy.

An inherent signature of the spin-glass phase is the chaotic behavior [41, 42, 43, 44, 45, 46, 47, 48] of the interaction at a given locality as a function of scale change, namely under consecutive renormalization-group transformations. This chaos is shown in Fig. 3.5 for a variety of dimensions, including the lower-critical dimension $d_c = 2.431$. For

each chaos, the Lyapunov exponent

$$\lambda = \lim_{n \rightarrow \infty} \frac{1}{n} \sum_{k=0}^{n-1} \ln \left| \frac{dx_{k+1}}{dx_k} \right| \quad (3.2)$$

where $x_k = J(ij)/\overline{|J|}$ at step k of the renormalization-group trajectory, measures the strength of the chaos, and is calculated and shown for the spatial dimensions in Fig. 3.5.

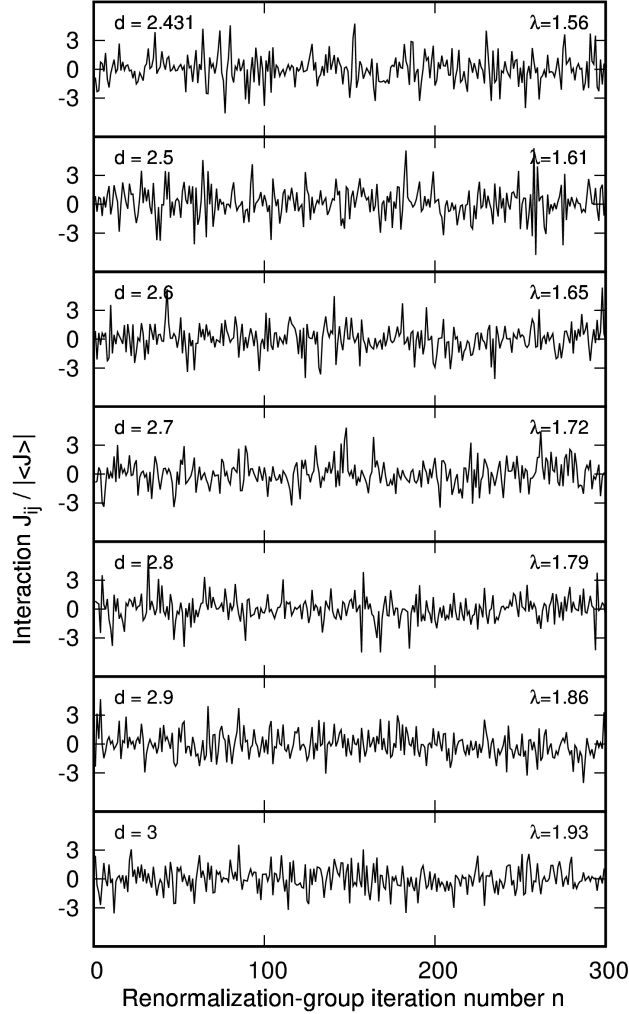


Figure 3.5: The chaotic renormalization-group trajectory of the interaction J_{ij} at a given location $\langle ij \rangle$, for various spatial dimensions between the lower-critical $d_c = 2.431$ and $d = 3$. Note that strong chaotic behavior, as also reflected by the shown calculated Lyapunov exponents λ , nevertheless continues as the spin-glass phase disappears at the lower-critical dimension d_c , as also seen in Fig. 3.6.

It is seen that the system shows strong chaos (positive Lyapunov exponent $\lambda = 1.56$) even at $d_c = 2.431$, namely at the brink of the disappearance of the spin-glass phase, after an essentially slow numerical evolution from the $d = 3$ value of $\lambda = 1.93$. This is in sharp contrast with the disappearance of the spin-glass phase, into a Mattis-gauge-transformed ferromagnetic phase, as frustration is gradually turned off microscopically, where chaos

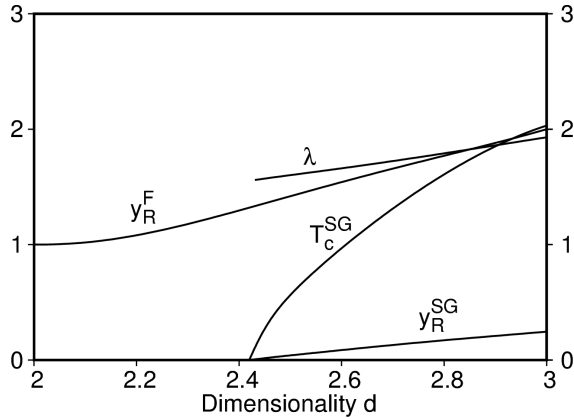


Figure 3.6: Spin-glass critical temperature T_c^{SG} at $p = 0.5$, spin-glass chaos Lyapunov exponent λ , spin-glass-phase runaway exponent y_R^{SG} and ferromagnetic-phase runaway exponent y_R^F , as a function of dimension d . Note that the ferromagnetic phase runaway exponent y_R^F correctly tracks $d - 1$.

gradually disappears and the Lyapunov exponent continuously goes to zero, as seen in Fig. 3.6 of Ref. [22]. As seen in Fig. 3.6, the Lyapunov exponent, shown continuously as a function of dimension, is essentially unaffected by the disappearance of the spin-glass phase and thus shows a discontinuity at d_c . The runaway exponent of the spin-glass phase, on the other hand, correctly goes to zero at d_c , as is expected by the renormalization-group flow structure. Also seen in Fig. 3.6 is the spin-glass critical temperature going to zero at d_c .

3.4. Conclusion

By quenched-randomly mixing local units of different spatial dimensionalities, we have studied Ising spin-glass systems on hierarchical lattices continuously in dimensionalities $1 \leq d \leq 3$. We have calculated the global phase diagram in temperature, antiferromagnetic bond concentration, and spatial dimensionality. We find that, as dimension is lowered, the spin-glass phase disappears at zero temperature at $d_c = 2.431$. Our system being a physically realizable system, this sets an upper limit to the lower-critical dimension of the Ising spin-glass phase. As dimension is lowered towards d_c , the spin-glass critical temperature continuously goes to zero. The Lyapunov exponent, measuring the strength of chaos, is on the other hand largely unaffected by the approach to d_c and shows a discontinuity to zero at d_c .

Chapter 4

CONCLUSION

In this thesis we have studied maximally random discrete-spin systems, and Ising spin-glass systems on hierarchical lattices continuously in dimensionalities $1 \leq d \leq 3$.

In Chapter 2, we have investigated discrete-spin systems with nearest-neighbor interactions, where we allowed each spin site to randomly favor one of the available states for its interaction with a nearest neighbor, thereby allowing the system to form both asymmetric and symmetric interactions and enabling maximal randomness throughout the system. We have found that such systems exhibit short-range disordering in the presence of a long-range order, and ultimately flow towards the ordered fixed point, at any non-infinite temperature, and for both integer and non-integer spatial dimensions for $d \gtrsim 1$. At order, the dominant interaction is any and only one of the $q \times q$ equally-weighted outcomes, thus maximally degenerate. The implacable long-range ordering is only belated at high temperatures, where the system spends many renormalization-group iterations near the infinite-temperature fixed point - a smeared transition into short-range disorder, likewise seen in the maxima of calculated specific heat diagrams. Keeping the temperature constant, this behavior is also observed if we approach $d = 1$ from above where we see increase in the high-temperature range of short-range disorder. The triumph of disorder only occurs at $d = 1$ where the system is disordered at any temperature, since the infinite-temperature fixed point becomes the sole attractor. We also considered the antiferromagnetic case ($J < 0$), and obtained quantitatively similar behavior.

In Chapter 3, by quenched-randomly mixing local units of different spatial dimensionalities, we have studied Ising spin-glass systems on hierarchical lattices continuously in dimensionalities $1 \leq d \leq 3$. We have calculated the global phase diagram in temperature, antiferromagnetic bond concentration, and spatial dimensionality. We find that, as dimension is lowered, the spin-glass phase disappears at zero temperature at $d_c = 2.431$.

Our system being a physically realizable system, this sets an upper limit to the lower-critical dimension of the Ising spin-glass phase. As dimension is lowered towards d_c , the spin-glass critical temperature continuously goes to zero. The Lyapunov exponent, measuring the strength of chaos, is on the other hand largely unaffected by the approach to d_c and shows a discontinuity to zero at d_c .

Bibliography

- [1] B. Nienhuis, A. N. Berker, E. K. Riedel, and M. Schick, Phys. Rev. Let. **43**, 737 (1979).
- [2] G. Delfino and E. Tartaglia, Phys. Rev. E **96**, 042137 (2017).
- [3] T. Çağlar and A. N. Berker, Phys. Rev. E **96**, 032103 (2017).
- [4] A. N. Berker and L. P. Kadanoff, J. Phys. A **13**, L259 (1980).
- [5] A. N. Berker and L. P. Kadanoff, J. Phys. A **13**, 3786 (1980).
- [6] E. Domany, J. L. van Hemmen, and K. Schulten (Eds.) *Models of Neural Networks*(Springer-Verlag, Berlin, 1991).
- [7] A. A. Migdal, Zh. Eksp. Teor. Fiz. **69**, 1457 (1975) [Sov. Phys. JETP **42**, 743 (1976)].
- [8] L. P. Kadanoff, Ann. Phys. (N.Y.) **100**, 359 (1976).
- [9] A. N. Berker and S. Ostlund, J. Phys. C **12**, 4961 (1979).
- [10] R. B. Griffiths and M. Kaufman, Phys. Rev. B **26**, 5022R (1982).
- [11] M. Kaufman and R. B. Griffiths, Phys. Rev. B **30**, 244 (1984).
- [12] N. Masuda, M. A. Porter, and R. Lambiotte, Phys. Repts. **716**, 1 (2017).
- [13] S. Li and S. Boettcher, Phys. Rev. A **95**, 032301 (2017).
- [14] P. Bleher, M. Lyubich, and R. Roeder, J. Mathematiques Pures et Appliquées **107**, 491 (2017).
- [15] H. Li and Z. Zhang, Theoretical Comp. Sci. **675**, 64 (2017).
- [16] J. Peng and E. Agliari, Chaos **27** 083108 (2017).

- [17] T. Nogawa, arXiv:1710.04014 [cond-mat.stat-mech](2017)
- [18] S. J. Sirca and M. Omladic, ARS Mathematica Contemporanea **13**, 63 (2017).
- [19] J. Maji, F. Seno, A. Trovato, and S. M. Bhattacharjee, J. Stat. Mech.: Theory Exp. 073203 (2017).
- [20] D. Yeşiltepe and A. N. Berker, Phys. Rev. Lett. **78**, 1564 (1997).
- [21] A. N. Berker and D. R. Nelson, Phys. Rev. B **19**, 2488 (1979).
- [22] E. Ilker and A. N. Berker, Phys. Rev. E **89**, 042139 (2014).
- [23] H. E. Stanley and T. A. Kaplan, Phys. Rev. Lett. **17**, 913 (1966).
- [24] H. E. Stanley, Phys. Rev. Lett. **20** 589 (1968).
- [25] D. P. Belanger, A. R. King, and V. Jaccarino, Phys. Rev. Lett. **48**, 1050 (1982).
- [26] H. Yoshizawa, R. A. Cowley, G. Shirane, R. J. Birgeneau, H. J. Guggenheim, and H. Ikeda, Phys. Rev. Lett. **48**, 438 (1982).
- [27] P.-z. Wong and J. W. Cable, Phys. Rev. B **28**, 5361 (1983).
- [28] A. N. Berker, Phys. Rev. B **29**, 5243 (1984).
- [29] M. Aizenman and J. Wehr, Phys. Rev. Lett. **62**, 2503 (1989).
- [30] M. Aizenman and J. Wehr, Phys. Rev. Lett. **64**, 1311(E) (1990).
- [31] M. S. Cao and J. Machta, Phys. Rev. B **48**, 3177 (1993).
- [32] A. Falicov, A. N. Berker, and S.R. McKay, Phys. Rev. B **51**, 8266 (1995).
- [33] S. Franz, G. Parisi, and M.A. Virasoro, J. Physique I **4**, 1657 (1994).
- [34] S. Boettcher, Phys. Rev. Lett. **95**, 197205 (2005).
- [35] A. Maiorano and G. Parisi, Proc. Natl. Acad. Sci. USA **115**, 5129 (2018).
- [36] C. Amoruso, E. Marinari, O. C. Martin, and A. Pagnani, Phys. Rev. Lett. **91**, 087201 (2003).
- [37] J.-P. Bouchaud, F. Krzakala, and O. C. Martin, Phys. Rev. B **68**, 224404 (2003).

- [38] M. Demirtaş, A. Tuncer, and A. N. Berker, *Phys. Rev. E* **92**, 022136 (2015).
- [39] S. Boettcher and S. Li, *Phys. Rev. A* **97**, 012309 (2018).
- [40] B. Atalay and A. N. Berker, *Phys. Rev. E* **97**, 052102 (2018).
- [41] S. R. McKay, A. N. Berker, and S. Kirkpatrick, *Phys. Rev. Lett.* **48**, 767 (1982).
- [42] S. R. McKay, A. N. Berker, and S. Kirkpatrick, *J. Appl. Phys.* **53**, 7974 (1982).
- [43] A. N. Berker and S. R. McKay, *J. Stat. Phys.* **36**, 787 (1984).
- [44] Z. Zhu, A. J. Ochoa, S. Schnabel, F. Hamze, and H. G. Katzgraber, *Phys. Rev. A* **93**, 012317 (2016).
- [45] W. Wang, J. Machta, and H. G. Katzgraber, *Phys. Rev. B* **93**, 224414 (2016).
- [46] L. A. Fernandez, E. Marinari, V. Martin-Mayor, G. Parisi, and D. Yllanes, *J. Stat. Mech.: Theory Exp.* 123301 (2016).
- [47] A. Billoire, L. A. Fernandez, A. Maiorano, E. Marinari, V. Martin-Mayor, J. Moreno-Gordo, G. Parisi, F. Ricci-Tersenghi, J. J. Ruiz-Lorenzo, *J. Stat. Mech.: Theory Exp.* 033302 (2018).
- [48] W. Wang, M. Wallin, and J. Lidmar, arXiv:1808.00886 [cond-mat.dis-nn] (2018).